COMMUNICATIONS CHEMISTRY

ARTICLE

DOI: 10.1038/s42004-018-0017-z OPEN

Carbon nanotubes and manganese oxide hybrid nanostructures as high performance fiber supercapacitors

Wei Gong[1], Bunshi Fugetsu[2], Zhipeng Wang[1], Ichiro Sakata[1,2], Lei Su[3], Xueji Zhang[3], Hironori Ogata[4], Mingda Li[5], Chao Wang[5], Ju Li[5], Josue Ortiz-Medina[6], Mauricio Terrones[6,7] & Morinobu Endo[6]

Manganese oxide (MnO_2) has long been investigated as a pseudo-capacitive material for fabricating fiber-shaped supercapacitors but its poor electrical conductivity and its brittleness are clear drawbacks. Here we electrochemically insert nanostructured MnO_2 domains into continuously interconnected carbon nanotube (CNT) networks, thus imparting both electrical conductivity and mechanical durability to MnO_2. In particular, we synthesize a fiber-shaped coaxial electrode with a nickel fiber as the current collector (Ni/CNT/MnO_2); the thickness of the CNT/MnO_2 hybrid nanostructured shell is approximately 150 μm and the electrode displays specific capacitances of 231 mF cm^{-1}. When assembling symmetric devices featuring Ni/CNT/MnO_2 coaxial electrodes as cathode and anode together with a 1.0 M Na_2SO_4 aqueous solution as electrolyte, we find energy densities of 10.97 μWh cm^{-1}. These values indicate that our hybrid systems have clear potential as wearable energy storage and harvesting devices.

[1] School of Engineering, The University of Tokyo, Bunkyo-ku, Tokyo 113-8656, Japan. [2] Policy Alternatives Research Institute, The University of Tokyo, Bunkyo-ku, Tokyo 113-0033, Japan. [3] Research Centre for Bioengineering and Sensing Technology, University of Science and Technology Beijing, Haidian District, Beijing 100083, China. [4] Graduate School of Science and Engineering, Hosei University, Koganei, Tokyo 184-8584, Japan. [5] Department of Nuclear Science and Engineering and Department of Materials Science and Engineering, Massachusetts Institute of Technology, 77 Massachusetts Avenue, Cambridge, MA 02139, USA. [6] Institute of Carbon Science and Technology, Shinshu University, 4-17-1 Wakasato, Nagano 380-8553, Japan. [7] Department of Physics, Department of Chemistry, Department of Materials Science and Engineering and Center for 2-Dimensional and Layered Materials, The Pennsylvania State University, University Park, PA 16802, USA. Correspondence and requests for materials should be addressed to B.F. (email: bunshifugetsu@pari.u-tokyo.ac.jp)

Fiber-shaped supercapacitors (FSCs) constitute a class of one-dimensional electrical devices for energy storage[1–3]. Their wearable nature, low weight, and high flexibility make them suitable for powering portable microelectromechanical devices[4–6] or other wearable electronic systems[7–11]. Similar to conventional planar- and cylindrical-shaped supercapacitors, FSCs store energy via either the electrical double layer (EDL) principle or the pseudo-capacitance mechanism[1]. For the EDL-based FSCs[7,10,12–17], energy density is governed by the overall capability of the absorbing electrolytes (cations and anions), by having active materials embedded within electrodes. For the pseudo-capacitive FSCs[4–6,8,9,18–21], on the other hand, the overall amount of the redox-active materials of the electrodes is key for determining the energy density. Purely EDL-based FSCs with carbon materials arranged as fibers and/or yarns have resulted in high power densities and enhanced cycling stabilities; their energy densities however are often limited to a few mF cm^{-1} [22–25]. Activated carbons, carbon nanotubes (CNTs), graphene, and reduced graphene oxide (rGO) have also been used as active materials for fabricating fiber-shaped and/or yarn-shaped electrodes.

Of the many outstanding achievements, an effort made by Liu et al.[26] is noteworthy: they built up a typical supercapacitor exhibiting 110 mF cm^{-1} energy density, which appears to be the highest value reported to date for purely EDL-based FSCs. The rGO being electrochemically deposited on nickel-coated multi-filament cotton yarns was also used as an active material. Its high energy density was attributed to the large surface area of rGO. As current collectors, nickel-coated cotton yarns were synthesized via electroless deposition[26], thus preserving high flexibility and the best electrical resistance has been optimized at *ca.* 1.3 Ω cm^{-1}, a value which is much higher than that of normal nickel fibers (*ca.* 5.1×10^{-2} Ω cm^{-1}).

For pseudo-capacitive FSCs, energy density values based on reversible redox interactions can be as high as many times that of purely EDL-based capacitors[1]. Therefore, the loading of the redox-active materials has been a challenge in the fabrication of

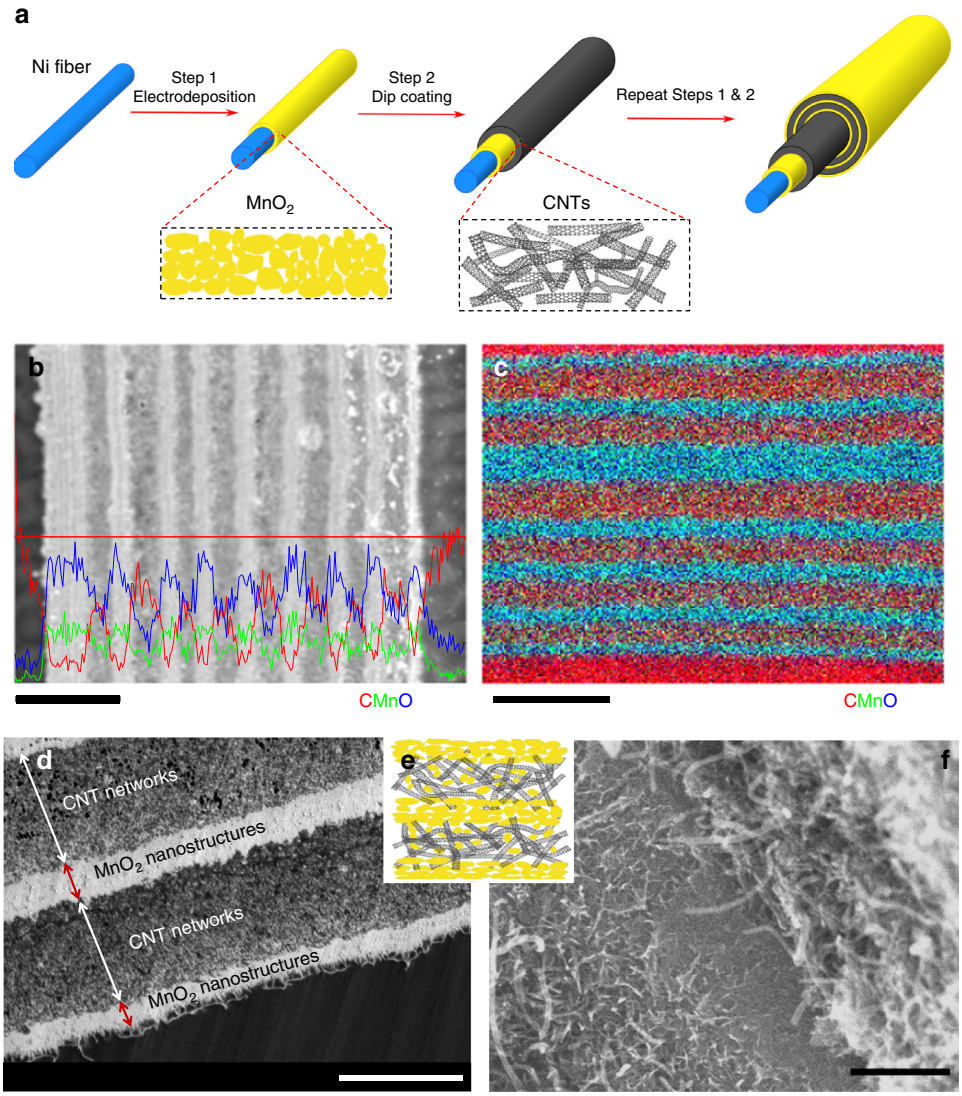

Fig. 1 Fabrication schemes and images of a CNT/MnO_2 hybrid nanostructured electrode. **a** Schematic illustration of the fabrication of a coaxial-shaped CNT/MnO_2 electrode with a Ni fiber as the current corrector. **b** Line-scan EDS data on a cross-section image of a typical CNT/MnO_2 hybrid nanostructured electrode (9-layered MnO_2 and 8-layered CNTs) showing C (carbon, red line), Mn (manganese, green line), and O (oxygen, blue line) atoms (scale bar, 2.5 μm). **c** EDS elemental mappings for C, Mn, and O, respectively (scale bar, 3 μm). **d** A cross-sectional SEM image (scale bar, 2 μm) obtained by polishing with a cross-section polisher. **e** Schematic illustration of the configuration of the CNT/MnO_2 hybrid nanostructures. **f** A cross-sectional SEM image of fracture end area of the CNT/MnO_2 hybrid nanostructures (scale bar, 250 nm)

the pseudo-capacitive FSCs. Redox-active materials, especially inorganic systems such as MnO_2, RuO_2, $Ni(OH)_2$, and $Co(OH)_2$, are highly brittle and exhibit poor electrical conductivity values[27]. In this context, Kim and co-workers[11,28] have recently reported an effective approach that is able to overcome both the brittleness and low electrical conductivity. In particular, manganese oxide (MnO_2) nanoparticles were uniformly deposited on a piece of a CNT sheet *via* drop casting a dispersion containing MnO_2 nanoparticles which was then twisted into bi-scrolled yarns. MnO_2 loading rate could be maximized up to 93 wt% while the CNT sheet based yarns retained excellent flexibility and mechanical durability. In this case, the maximum energy density reported was 60.6 mF cm^{-1}. Therefore, wrapping MnO_2 with CNT sheet constitutes an alternative to maximize the loading ratio of the redox-active materials. However, the full activation of MnO_2 is not possible via physically wrapping the redox-active materials with CNT sheets.

Hybrid structures resembling tissue cells and capillaries in living organisms inspired our studies; one could visualize MnO_2 domains as tissue cells and CNT networks as capillaries. In this study we describe the synthesis of CNT/MnO_2 hybrid nanostructures by electrochemically inserting nanostructured MnO_2 domains into continuously interconnected CNT networks. These CNT/MnO_2 hybrid nanostructures are self-conducting, and the transfer of electrons during charge and discharge can be achieved rapidly; this occurs almost independently of the thickness of the CNT/MnO_2 system. We also fabricate different coaxial fiber-shaped electrodes using CNT/MnO_2 hybrid nanostructures as the pseudo-capacitive materials. The fiber core, which functions as current collectors can be either metal wires/fibers or carbon fibers. As the pseudo-capacitive materials of FSCs, our CNT/MnO_2 hybrid nanostructures can be loaded up to a maximum thicknesses of *ca.* 150 μm, while both the Faradic efficiency and the mechanical properties are retained with excellent performance. In particular, we obtain specific capacitances of 231 mF cm^{-1}, which is about four times the value reported for the CNT-sheet-wrapped MnO_2 electrodes[11]. We believe these results pave the way to establish new assemblies with a high impact in energy-related applications.

Results

Synthesis and characterization of fiber-shaped Ni/CNT/MnO_2 electrodes. Figure 1a schematically illustrates the process for fabricating a coaxial fiber-shaped CNT/MnO_2 hybrid nanostructured electrode, in which a nickel fiber (O.D. 200 μm) was used as the current collector (denoted as Ni/CNT/MnO_2 electrode). Two key features need to be following during preparation: (i) the interconnected CNT networks with thicknesses of *ca.* 300 nm were prepared by "dipping and drying", and (ii) nanostructured MnO_2 domains were electrochemically deposited within the CNT networks by cyclic voltammetry (CV). The thickness of the MnO_2 domains was precisely controlled by controlling CV scan rate. These two steps (step (i) and step (ii)) were repeated for several cycles until the CNT/MnO_2 hybrid nanostructures with a desirable thickness were achieved. For example, a Ni/CNT/MnO_2 electrode carrying CNT/MnO_2 with a total thickness of 9.1 μm was prepared after 9 cycles of MnO_2 deposition at a CV scan rate of 50 mV s^{-1} and 8 cycles for depositing the CNT networks. Energy dispersive spectroscopy (EDS) analysis of carbon (contained in CNTs), manganese, and oxygen (present in MnO_2) are shown in Supplementary Figure 1a-c. The data indicated that the CNT/MnO_2 hybrid nanostructures are indeed constructed by MnO_2 and CNTs. Elemental EDS line scans (Fig. 1b) are overlapped with element mappings of carbon, manganese, and oxygen (Fig. 1c), and scanning electron microscopy (SEM) images (Fig. 1d). These provided a clear composition of the CNT/MnO_2 hybrid nanostructures. It is clear that MnO_2 domains have penetrated into the CNT networks (Fig. 1e, f). The initial thickness of CNT networks was 300–400 nm but it expanded to 1.1–1.3 μm after the electrochemical deposition of the nanostructured MnO_2 domains. In our experiments, manganese acetate dissolved in 0.1 M sodium sulfate aqueous solution was used as the bath for electrodepositing the nanostructured MnO_2 domains. In particular, manganese ions (Mn^{2+}) penetrated into the whole CNT networks via self-diffusion. The expansion of the CNT networks from 300–400 nm to 1.1–1.3 μm could be due to the formation of the nanostructured MnO_2 nanoparticles within the CNT networks, similar to previous observations[5,29]. A schematic illustration is shown in Fig. 1e, depicting the distribution of CNT/MnO_2 hybrid nanostructures. While MnO_2 domains were densely packed, the CNT networks exhibited plenty of entangled cavities (Fig. 1d, f). EDS mapping for sodium (cation of electrolyte, Na_2SO_4) was also recorded (Supplementary Figure 1d). In this case, sodium ions were uniformly distributed through the CNT/MnO_2 hybrid nanostructures, thus indicating a high accessibility of the electrolyte. Supplementary Figure 1e shows an SEM image of a cross-sectional area at low resolution. Neither the physically over-wrapping method[11] nor the "layer-by-layer" method[30] are applicable for depositing MnO_2 nanostructures into the heavily interconnected CNT networks we produced with high electrical conductivity values.

As mentioned above, the thickness of the MnO_2 domains deposited electrochemically depends on the CV scan rate. For example, by reducing the CV scan rate and increasing the deposition time, thick nanostructured MnO_2 domains can be deposited. The electrochemical conditions used in this study are shown in Supplementary Figure 2. It is noteworthy that our CNT/MnO_2-based electrodes showed electrochemical properties that were superior when compared to those based only on MnO_2 (Supplementary Figure 2a-d), especially for the electrodes constructed using low CV scan rates (10, 5, 2 mV s^{-1}). Furthermore, a huge difference in the specific capacitances was observed (Supplementary Figure 2e). For the CNT/MnO_2 electrodes prepared at CV scan rates of 2 mV s^{-1}, specific capacitances of 9902 μF cm^{-1} were achieved, whereas a CNT-free MnO_2 electrode showed values of 1803 μF cm^{-1}. SEM images (Supplementary Figure 3) revealed cracked structures for the CNT-free MnO_2-based electrodes prepared at CV scan rates of ≤20 mV s^{-1} (Supplementary Figure 3a-c). The same situation was observed in previous studies[31]. For our CNT/MnO_2 hybrid nanostructures, as can be seen from the SEM images (Supplementary Figure 3d-f), the MnO_2 domains were heavily covered by interconnected CNT networks (Supplementary Figure 3g-i), and the transfer of electrons among all the MnO_2 domains can rapidly occur through the CNT networks. The nanostructured MnO_2 domains resemble tissue cells while the heavily interconnected CNT networks are analogs of capillaries. This unique hybrid architecture enabled both high electrochemical reactivity and robust mechanical properties. The thickest CNT/MnO_2 hybrid nanostructure we studied was 149 μm thick, and it was obtained after 10 electrochemical cycles for depositing MnO_2 at a CV scan rate of 2 mV s^{-1}, and 9 cycles for the CNT deposition. The actual amount of MnO_2 being loaded in the ten-layered CNT/MnO_2 hybrid electrode was estimated to be 2.06 mg cm^{-1}. The capacitance values for different cycles for depositing MnO_2 and CNT networks at CV scan rates of 2, 5, 10, and 50 mV s^{-1} are shown in the Supplementary Figure 4a. The specific capacitance for all electrodes was proportional to the CNT/MnO_2 thickness. The presence of CNT networks allowed MnO_2 domains to have full contributions to the capacitance (Supplementary Figure 4b).

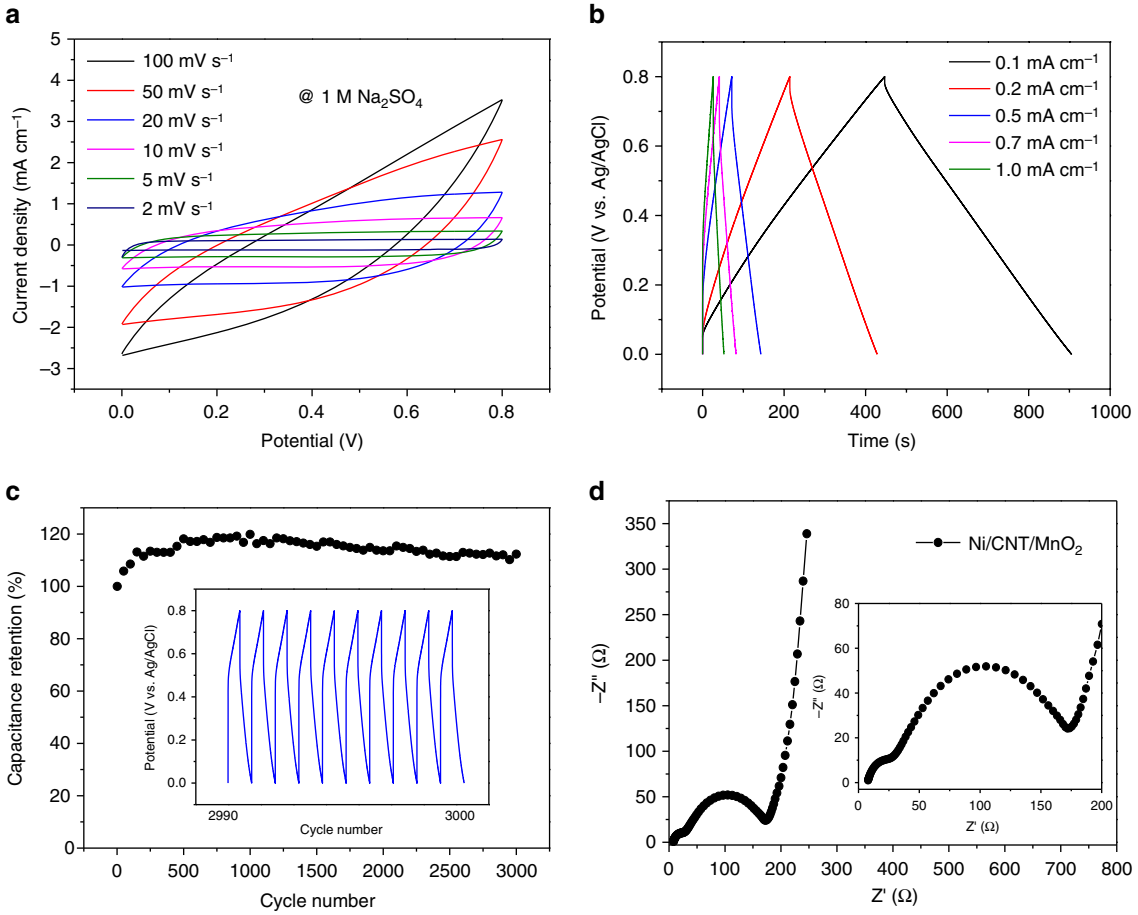

Fig. 2 Electrochemical performance of a Ni/CNT/MnO_2 electrode. **a** CV curves measured at different scan rates in 1.0 M Na_2SO_4. **b** Galvanostatic charge/discharge curves at different current densities. **c** Cycling performance at 2 mA cm^{-1}; inset: galvanostatic charge/discharge curves from the 2990th to 3000th cycle. **d** EIS spectrum of the same Ni/CNT/MnO_2 electrode; inset: the high-frequency region (Ni/CNT/MnO_2 electrode, 9-layerd MnO_2 and 9-layered CNTs obtained using CV scan rate at 10 mV s^{-1}, thickness, 48 μm)

As mentioned above, the ratio of MnO_2 within the CNT/MnO_2 hybrid nanostructures varies as a function of the CV scan rate, estimated to be 49.39 wt%, 66.13 wt%, 82.99 wt%, 90.71 wt%, 95.13 wt%, and 97.99 wt% for scan rates of 100, 50, 20, 10, 5, and 2 mV s^{-1}, respectively. These values were calculated from EDS analysis for each CNT/MnO_2 sample. Thus, for the 2 mV s^{-1} deposited shell, the weight and capacitance of active material are both dominated by MnO_2, even though CNT plays important role for mechanical support and electron percolation.

Nanostructured MnO_2 domains embedded within CNT/MnO_2 hybrids produced via electrochemical deposition exhibit the δ-crystalline phase, confirmed by X-ray diffraction (XRD) patterns (Supplementary Figure 5). As redox-active materials, δ- and α-crystalline nanostructured MnO_2 always resulted in the best capacitance values (γ, λ, and then β)[32,33]. The MnO_2 domains involved in the CNT/MnO_2 hybrid nanostructures were built up by aggregating MnO_2 nanoparticles. The average grain size of MnO_2 nanoparticles were in the range of 5–30 nm, and strongly dependent on the CV scan rate.

Mechanism of energy storage for the CNT/MnO_2 hybrid nanostructures. Similar to MnO_2-based pseudo-capacitive materials, our CNT/MnO_2 hybrid nanostructures store energy *via* both redox interactions and ion intercalation/deintercalation. Equation (1) describes the chemical description for the energy storing mechanism[34,35]:

$$MnO_2 + E^+ + e^- \rightleftharpoons MnOOE, \quad (1)$$

where E^+ denotes the cations of electrolyte. Mn(IV) in MnO_2 displays a high oxidation state, having a higher potential than that of E^+ during charging the supercapacitor. In other words, Eq. (1) can be rearranged in to Eq. (2), where E^+ remained largely as cations but being electrically balanced by electrons, e^-:

$$Mn(IV)O_2 + E^+ + e^- \rightleftharpoons [Mn(III)OO]^- \ldots E^+, \quad (2)$$

where $[Mn(III)OO]^- \ldots E^+$ denotes an electrically induced intermediated state which stores electrons, i.e., energies via redox and ion-intercalation interactions. However, due to the very poor electrical conductivity of MnO_2, the formation of $[Mn(III)OO]^- \ldots E^+$, i.e., the redox and intercalation interactions, is restricted to a very thin MnO_2 subsurface (*ca.* 420 nm[34]). Our CNT/MnO_2 hybrid nanostructures, as can be seen from Fig. 1d, is novel and desirable since it is able to maximize the formation of $[Mn(III)OO]^- \ldots E^+$. It is also noteworthy that the thickness of MnO_2 domains can be precisely tuned at *ca.* 500 nm by controlling the CV scan rate and, moreover, electrons involved in $[Mn(III)OO]^- \ldots E^+$ can be effectively delivered via the CNT networks. In other words, the CNT networks functioned as "electrical capillaries" which deliver electrons to nanostructured MnO_2 domains. High capacitances can be achieved by increasing the overall thickness of MnO_2 domains within the CNT/MnO_2 hybrid nanostructures.

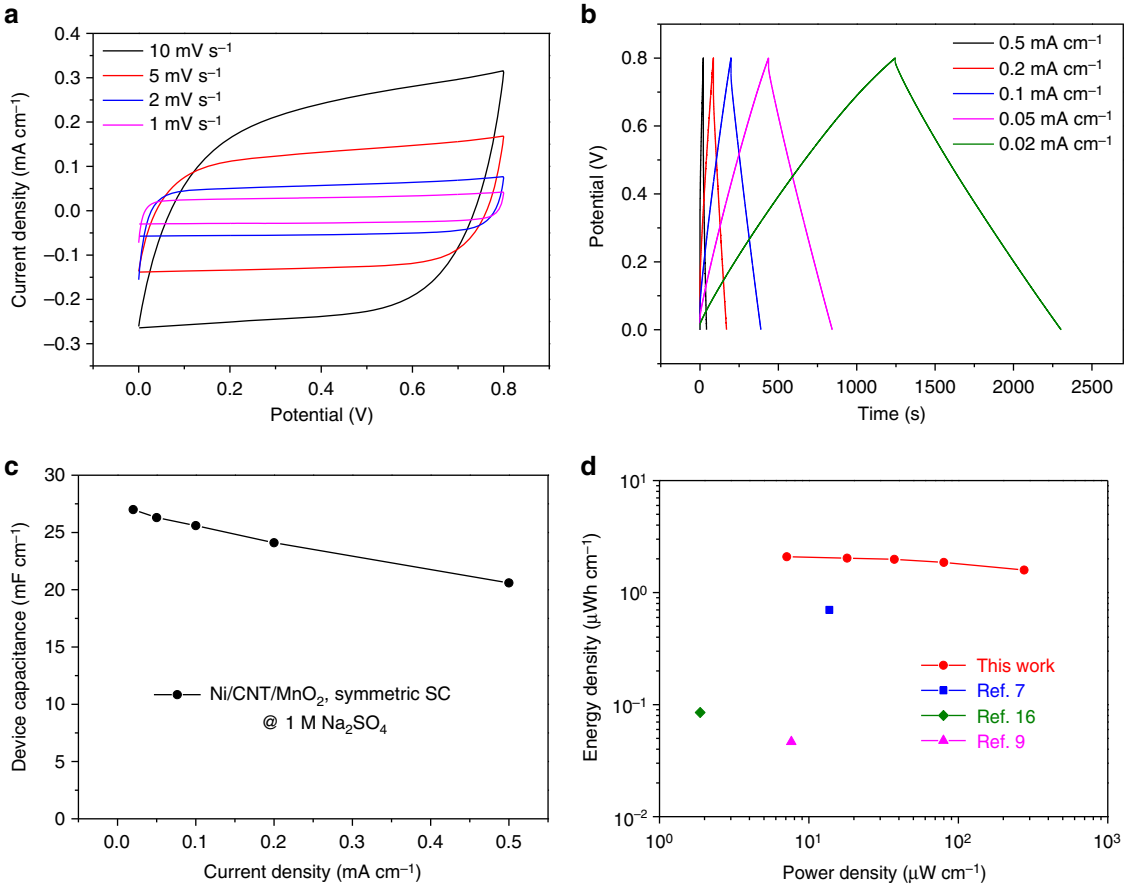

Fig. 3 Electrochemical performance of a symmetric fiber-shaped supercapacitor device. **a** CV curves of the symmetric supercapacitor device (cathode and anode: Ni/CNT/MnO_2, 9-layered MnO_2 and 9-layered CNTs, total thickness, 48 μm) measured at various scan rates in 1.0 M Na_2SO_4. **b** Galvanostatic charge/discharge curves and **c** device capacitance of the symmetric supercapacitor device at various current densities. **d** Energy density and power density of the same supercapacitor device compared with typical published data on the fiber-shaped supercapacitor devices

Supplementary Figure 6 shows typical plots of the specific capacitance *vs.* thickness of the CNT/MnO_2 hybrid nanostructures. The Ni/CNT/MnO_2 electrode having a 149 μm thick CNT/MnO_2 shell with 2.06 mg cm^{-1} MnO_2 loading exhibited capacitances of 231.2 mF cm^{-1}. The best reported data for the specific capacitance in MnO_2 using CNT sheets was 60.6 mF cm^{-1}, which is about one-fourth the value of the performance of our CNT/MnO_2 multi-layered structure. Figure 2 shows CV curves (Fig. 2a), galvanostatic charge/discharge curves (Fig. 2b), cycling performance (Fig. 2c), and electrochemical impedance spectroscopy (EIS) spectra (Fig. 2d) for the coaxial Ni/CNT/MnO_2 electrodes. All experiments were carried out using a three-electrode system in a 1.0 M Na_2SO_4 solution. The Ni/CNT/MnO_2 hybrid nanostructured electrode used in Fig. 2 was electrochemically prepared using CV scan rates of 10 mV s^{-1}, and the overall thickness of the CNT/MnO_2 hybrid nanostructure was about 48 μm. Quasi-rectangular-shaped CV curves were observed when the CV scan rates ranged from 2 mV s^{-1} to 100 mV s^{-1} (Fig. 2a), as well as symmetrically shaped galvanostatic charge/discharge curves (Fig. 2b), thus indicating the presence of an ideal pseudocapacitive material[29,36]. The specific capacitance *vs.* current densities for this Ni/CNT/MnO_2 electrode was calculated based on the galvanostatic charge/discharge curves. It was found to be 51.3, 49.1, 44.1, 37.5, and 36.2 mF cm^{-1} for current densities of 0.1, 0.2, 0.5, 0.7, and 1.0 mA cm^{-1}, respectively. The specific capacitance in weight of a 10-layered (CV rate for electrochemical deposition, 10 mV s^{-1}) CNT/MnO_2 hybrid electrode was calculated to be 236.5 F g^{-1} at a current density of 0.1 mA cm^{-1} by the mass of CNT/MnO_2 hybrid nanostructuresd shell. Long charge/discharge cycling tests were performed at a current density of 2 mA cm^{-1}, and the electrochemical stability of the CNT/MnO_2 hybrid nanostructures remained nearly constant even after 3000 cycles (Fig. 2c). We also measured the diameter of the electrode after certain cycles of charging and discharging processes; changes were not observed, indicating the excellent durability of the CNT/MnO_2 hybrid electrode. The CNT/MnO_2 hybrid electrode remained stable while the working potential for the supercapacitor ranged from 0 V to 0.8 V (*vs.* Ag/AgCl). In the EIS measurements, the Nyquist plots (Fig. 2d) showed a vertical line in a low-frequency region and the low equivalent series resistance was calculated to be 6.8 Ω cm^{-1}.

Symmetric supercapacitor devices. Two-electrode-type supercapacitors were assembled and the typical electrochemical responses are shown in Fig. 3. Cathode and anode consisted of a single piece of a Ni/CNT/MnO_2 fiber having an identical shell thickness at around 48 μm and lengths of 1.15 cm; a 1.0 M Na_2SO_4 aqueous solution was used as the electrolyte. Interestingly, this device gives quasi-rectangular-shaped CV curves (Fig. 3a) and symmetrically shaped galvanostatic charge/discharge curves (Fig. 3b), indicating excellent capacitive performances. Cell linear capacitance remained at 76.3% (from 27.0 to 20.6 mF cm^{-1}), even as the current density increased from 0.02 to 0.5 mA cm^{-1} (Fig. 3c). Energy density and power density of this two-electrode device were calculated to be 2.09 μWh cm^{-1} and

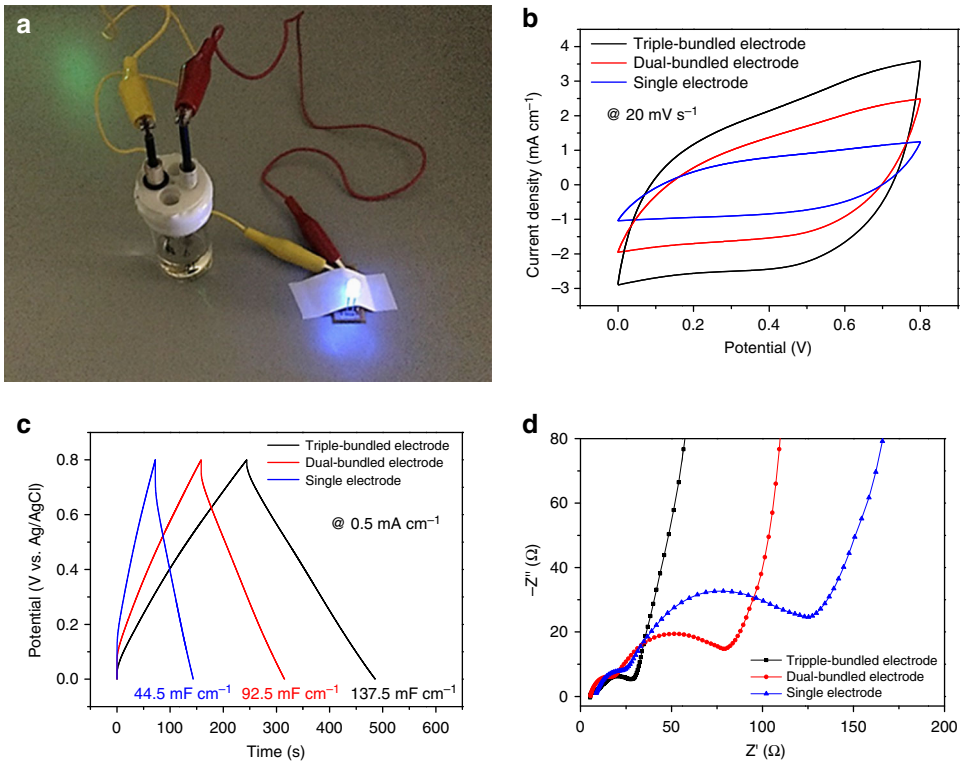

Fig. 4 Assembly of bundled Ni/CNT/MnO_2 electrodes for a supercapacitor device. **a** A digital photograph of a light-emitting diode (LED) powered by a triple-bundled two-electrode type of a symmetric supercapacitor device. **b** CV curves, **c** galvanostatic charge/discharge curves and **d** EIS spectra of a single, dual-, and triple-bundled Ni/CNT/MnO_2 electrode (9-layered MnO_2 and 9-layered CNTs, the total thickness is 48 μm)

7.11 μW cm^{-1}, respectively, at 0.02 mA cm^{-1}, and 1.59 μWh cm^{-1} and 275.6 μW cm^{-1}, for current densities of 0.5 mA cm^{-1} (Fig. 3d). Typical data on cell energy density and power density reported by other groups[7,9,16], are also given in Fig. 3d for comparison. Our CNT/MnO_2 hybrid nanostructures clearly show the best performance. Finally, two-electrode devices using Ni/CNT/MnO_2 electrodes having the maximum CNT/MnO_2 shell thickness (149 μm) resulted in energy densities of 10.97 μWh cm^{-1}, which, to the best of our knowledge, are the best data on the MnO_2-based FSCs reported hitherto. Energy density has been further enhanced by using bundled Ni/CNT/MnO_2 fibers as electrodes (cathode and anode). In this context, a symmetrical supercapacitor with a triple-bundled Ni/CNT/MnO_2 fiber (three strands of the 1.15-cm long Ni/CNT/MnO_2 fibers were bundled in parallel and were then used as both cathode and anode) as electrodes was assembled. Surprisingly, this was capable of powering a light-emitting diode (LED; Fig. 4a). Note here that three micro-supercapacitor devices connected in parallel were also capable of powering the LED (Supplementary Figure 7). From the CV (Fig. 4b) and galvanostatic charge/discharge curves (Fig. 4c), the capacitance was enhanced nearly twice and three times when the dual and the triple-bundled Ni/CNT/MnO_2 electrodes were used. The measured resistance (Fig. 4d) was 62.5 Ω, 37.5 Ω, and 12.5 Ω, for the single, dual-bundled, and the triple-bundled electrodes, respectively. In other words, bundled Ni/CNT/MnO_2 electrodes result in high energy densities and high power densities, and also lower the internal resistance values of the pseudo-capacitive materials.

Discussion

It is clear that our fiber supercapacitors are potentially capable of driving wearable electronic devices. We established a novel CNT/MnO_2 hybrid nanostructured material that resembles tissue cells and capillaries. In our case, CNT networks entangle within nanostructured MnO_2 domains, thus allowing electrons to be injected effectively via these conducting CNT networks. Pseudo-capacitive domains have been activated via Faradic and the intercalation/deintercalation interactions, and the capability for storing energy therefore has been enhanced. Moreover, the self-conducting properties of our CNT/MnO_2 hybrid nanostructures enabled us to increase the absolute energy density *via* the maximized loading rate of MnO_2. The bending stability of the electrode depends entirely on the properties of the current collectors. CNT/MnO_2 hybrid electrodes with carbon fibers as current correctors showed superior bending stabilities; they were able to bend 360 degrees while the electrochemical performance remained unchanged. Other combinatorial nanostructures, such as CNT/TiO_2, CNT/RuO_2, CNT/PbO_2, CNT/$Ni(OH)_2$, and CNT/$Co(OH)_2$, are also possible via the electrochemical-deposition/CNT network formation methodology. We believe that our results pave the way to the design and development of novel wearable energy storage devices.

Methods

Preparation of aqueous dispersions containing mono-dispersed CNTs. As-grown, entangled multi-walled CNT powders (NC7000^{TM}), were purchased from Nanocyl S.A. (Belgium). They were further dispersed into aqueous suspensions via the following steps: (i) 40 g of the as-purchased CNT powders were pre-dispersed into 1000 ml deionized water using a ball mill system (Multi Lab DYNO-Mill, 0.6 mm zirconium beads), (ii) 10 g of sodium cholate (Wako Chemicals) was then introduced and the slurry was then ball milled for about 50 min, (iii) 5.0 g of Polyvinylpyrrolidone (PVP) (Wako Chemicals) and 2.0 g of hydroxypropyl cellulose (Wako Chemicals) were introduced and the slurry was further ball milled till the CNTs disperse individually. Degrees of dispersion (D90 < 60 nm) were confirmed by a series of size distribution analysis using a dynamic light scattering analyzer (HORIBA Dynamic Light Scattering Particle Size Analyzer LB-550). A typical SEM image showing CNTs being dispersed individually is given in Supplementary Figure 8. Cholate functioned as the dispersing agent while PVP and hydroxypropyl cellulose functioned as the stabilizers.

Preparation of the Ni/CNT/MnO_2 electrodes. Nanostructured MnO_2 domains were anodically electrodeposited onto CNT networks via a cyclic voltammetry. A Ni mono-fiber (diameter, 200 μm) was used as the working electrode, a platinum foil as the counter electrode, and an Ag/AgCl electrode as the reference electrode. The Ni fiber was immersed into an aqueous solution containing 0.1 M $Mn(Ac)_2$ and 0.1 M Na_2SO_4. Cyclic voltammograms were recorded between 0.4 and 1.4 V (*vs.* Ag/AgCl) at a certain scan rate (from 2 to 100 mV s^{-1}) for 1 cycle. After electrodepositing the nanostructured MnO_2 domains, the Ni/MnO_2 electrode was rinsed in deionized water and then dried at room temperature. The Ni/MnO_2 electrode was dipped into the mono-dispersed CNT suspension for 10 s and then rapidly removed. Subsequently, the Ni/CNT/MnO_2 electrode was dried using a heat gun. After drying, the Ni/CNT/MnO_2 electrode was subjected to surfactant/stabilizer removal by washing with abundant ethanol and deionized water, and dried at room temperature. The two steps were repeated several times until desirable Ni/CNT/MnO_2 hybrid nanostructured electrodes were obtained. Four 10-layered CNT/MnO_2 hybrid electrodes (CV scan rate for electrochemical deposition, 10 mV s^{-1}) were prepared under identical experimental conditions and the energy density of each electrode was measured. The standard deviation ($n = 4$) was found to be 5.7%, indicating the CNT/MnO_2 hybrid electrodes are reproducible.

Assembly of the symmetric supercapacitors. Two Ni/CNT/MnO_2 hybrid nanostructured electrodes were placed parallel and *ca.* 500 μm apart, then fixed with tape and inserted into a flexible plastic tube filled with a 1.0 M Na_2SO_4 aqueous solution. The tube was finally sealed with epoxy resin to prepare the symmetric devices. One end of each electrode was connected to a 180 μm diameter Cu wire using silver paste for electrochemical performance measurements.

Characterization. The materials were characterized by XRD pattern (R-AXIS RAPID-SH, Rigaku) using a Mo radiation (Kα, λ = 0.071069 nm), field emission SEM (Hitachi SU-8020) equipped with an energy-dispersive X-ray spectroscopy (HORIBA X-Max) and SEM (JEOL JSM-6390, Japan). The cross-sectioned electrodes were prepared using a cross-section polisher (CP, JEOL SM-09010). All electrochemical measurements including CV curves, galvanostatic charge/discharge curves, EIS (that was obtained with a sinusoidal potential excitation of 5 mV in the frequency range from 100 kHz to 0.01 Hz), and cycling performance measurements were carried out using an electrochemical workstation (CHI 760E, CH Instruments). The electrochemical performance of the electrode materials was measured in a three-electrode system with 1.0 M Na_2SO_4 electrolyte solution. Electrode materials, a platinum foil, and an Ag/AgCl electrodes were used as working electrodes, counter electrodes, and reference electrodes, respectively. The electrochemical performance of the symmetric supercapacitors was evaluated in a two-electrode system. Two symmetry fiber electrodes of the same length (1.15 cm) and from the same synthesis batch were immersed into a beaker containing 1.0 M Na_2SO_4 solution, with a distance of about 10 mm.

Calculation of the electrochemical performances. The specific linear capacitance of the single electrode-based pseudo-capacitive material (C_l) in a three-electrode cell was calculated from galvanostatic charge/discharge curves, according to the following equation[7]:

$$C_l = \frac{I \times \Delta t}{l \times \Delta V}, \tag{3}$$

where I denotes the constant discharge current; Δt denotes the time for a full discharge; l is the length of pseudo-capacitive electrode; and ΔV is the voltage drop on discharge (excluding the V_{drop}).

The capacitance of the supercapacitor device (C_{cell}) in a two-electrode cell was calculated from their galvanostatic charge/discharge curves at different current densities based on the following equation[14]:

$$C_{cell} = i/(dV/dt), \tag{4}$$

where i is the discharging current and dV/dt is the slope of the discharge curve.

The device linear capacitances of the FSCs ($C_{cell,l}$) was calculated according to the following equation:

$$C_{cell,l} = C_{cell}/l, \tag{5}$$

where l refers to the device length of the FSCs.

The linear energy density of the FSCs ($E_{cell,l}$) was obtained from the following equation:

$$E_{cell,l} = C_{cell,l}\Delta E^2/(2 \times 3600), \tag{6}$$

where ΔE is the operating voltage window in volts.

The linear power density of the FSCs ($P_{cell,l}$) was calculated from the galvanostatic curves at different charge/discharge current densities by using the following equation:

$$P_{cell,l} = E_{cell,l} \times 3600/t_{discharge}, \tag{7}$$

where $t_{discharge}$ is the discharge time.

The overall capacitance of the CNT/MnO_2 hybrid electrode increased proportionally as the length of the electrode increased. Due to the limitation of the surface area of the counter electrode, the maximum length of the CNT/MnO_2 hybrid electrode prepared in this study was restricted to 5.2 cm.

Data availability. The data that support the findings of this study are available from the corresponding author upon request.

Received: 14 November 2017 Accepted: 9 February 2018
Published online: 05 April 2018

References

1. Yu, D. et al. Emergence of fiber supercapacitors. *Chem. Soc. Rev.* **44**, 647–662 (2015).
2. Jost, K., Dion, G. & Gogotsi, Y. Textile energy storage in perspective. *J. Mater. Chem. A* **2**, 10776–10787 (2014).
3. Cai, X., Peng, M., Yu, X., Fu, Y. & Zou, D. Flexible planar/fiber-architectured supercapacitors for wearable energy storage. *J. Mater. Chem. C* **2**, 1184–1200 (2014).
4. Lee, J. A. et al. Ultrafast charge and discharge biscrolled yarn supercapacitors for textiles and microdevices. *Nat. Commun.* **4**, 1970 (2013).
5. Choi, C. et al. Flexible supercapacitor made of carbon nanotube yarn with internal pores. *Adv. Mater.* **26**, 2059–2065 (2014).
6. Xiao, X. et al. Fiber-based all-solid-state flexible supercapacitors for self-powered systems. *ACS Nano* **6**, 9200–9206 (2012).
7. Le, V. T. et al. Coaxial fiber supercapacitor using all-carbon material electrodes. *ACS Nano* **7**, 5940–5947 (2013).
8. Yu, N. et al. High-performance fiber-shaped all-solid-state asymmetric supercapacitors based on ultrathin MnO_2 nanosheet/carbon fiber cathodes for wearable electronics. *Adv. Energy Mater.* **6**, 1501458 (2016).
9. Xu, P. et al. Stretchable wire-shaped asymmetric supercapacitors based on pristine and MnO_2 coated carbon nanotube fibers. *ACS Nano* **9**, 6088–6096 (2015).
10. Kou, L. et al. Coaxial wet-spun yarn supercapacitors for high-energy density and safe wearable electronics. *Nat. Commun.* **5**, 3754 (2014).
11. Choi, C. et al. Improvement of system capacitance via weavable superelastic biscrolled yarn supercapacitors. *Nat. Commun.* **7**, 13811 (2016).
12. Jiang, W. et al. Space-confined assembly of all-carbon hybrid fibers for capacitive energy storage: realizing a built-to-order concept for micro-supercapacitors. *Energy Environ. Sci.* **9**, 611–622 (2016).
13. Chen, T., Hao, R., Peng, H. & Dai, L. High-performance, stretchable, wire-shaped supercapacitors. *Angew. Chem. Int. Ed.* **54**, 618–622 (2015).
14. Yu, D. et al. Scalable synthesis of hierarchically structured carbon nanotube-graphene fibres for capacitive energy storage. *Nat. Nanotechnol.* **9**, 555–562 (2014).
15. Yang, Z., Deng, J., Chen, X., Ren, J. & Peng, H. A highly stretchable, fiber-shaped supercapacitor. *Angew. Chem. Int. Ed.* **52**, 13453–13457 (2013).
16. Ren, J., Bai, W., Guan, G., Zhang, Y. & Peng, H. Flexible and weaveable capacitor wire based on a carbon nanocomposite fiber. *Adv. Mater.* **25**, 5965–5970 (2013).
17. Fu, Y. et al. Fiber supercapacitors utilizing pen ink for flexible/wearable energy storage. *Adv. Mater.* **24**, 5713–5718 (2012).
18. Li, M., Zu, M., Yu, J., Cheng, H. & Li, Q. Stretchable fiber supercapacitors with high volumetric performance based on buckled MnO_2/oxidized carbon nanotube fiber electrodes. *Small* **13**, 1602994 (2017).
19. Choi, C. et al. Elastomeric and dynamic MnO_2/CNT core-shell structure coiled yarn supercapacitor. *Adv. Energy Mater.* **6**, 1502119 (2016).
20. Yu, Z. & Thomas, J. Energy storing electrical cables: integrating energy storage and electrical conduction. *Adv. Mater.* **26**, 4279–4285 (2014).
21. Yu, D. et al. Controlled functionalization of carbonaceous fibers for asymmetric solid-state micro-supercapacitors with high volumetric energy density. *Adv. Mater.* **26**, 6790–6797 (2014).
22. Choi, C. et al. Microscopically buckled and macroscopically coiled fibers for ultra-stretchable supercapacitors. *Adv. Energy Mater.* **7**, 1602021 (2017).
23. Ren, J. et al. Twisting carbon nanotube fibers for both wire-shaped micro-supercapacitor and micro-battery. *Adv. Mater.* **25**, 1155–1159 (2013).

24. Meng, Y. et al. All-graphene core-sheath microfibers for all-solid-state, stretchable fibriform supercapacitors and wearable electronic textiles. *Adv. Mater.* **25**, 2326–2331 (2013).
25. Chen, X. et al. Novel electric double-layer capacitor with a coaxial fiber structure. *Adv. Mater.* **25**, 6436–6441 (2013).
26. Liu, L., Yu, Y., Yan, C., Li, K. & Zheng, Z. Wearable energy-dense and power-dense supercapacitor yarns enabled by scalable graphene-metallic textile composite electrodes. *Nat. Commun.* **6**, 7260 (2015).
27. Wang, G., Zhang, L. & Zhang, J. A review of electrode materials for electrochemical supercapacitors. *Chem. Soc. Rev.* **41**, 797–828 (2012).
28. Lima, M. et al. Biscrolling nanotube sheets and functional guests into yarns. *Science* **331**, 51–55 (2011).
29. Chou, S. L., Wang, J. Z., Chew, S. Y., Liu, H. K. & Dou, S. X. Electrodeposition of MnO_2 nanowires on carbon nanotube paper as free-standing, flexible electrode for supercapacitors. *Electrochem. Commun.* **10**, 1724–1727 (2008).
30. Zheng, H. et al. Layer-by-layer assembly and electrochemical properties of sandwiched film of manganese oxide nanosheet and carbon nanotube. *Carbon* **47**, 1534–1542 (2009).
31. Chen, Y. C. et al. Highly flexible supercapacitors with manganese oxide nanosheet/carbon cloth electrode. *Electrochim. Acta* **56**, 7124–7130 (2011).
32. Brousse, T. et al. Crystalline MnO_2 as possible alternative to amorphous compounds in electrochemical supercapacitors. *J. Electrochem. Soc.* **153**, A2171–A2180 (2006).
33. Devaraj, S. & Munichandraiah, N. Effect of crystallographic structure of MnO_2 on its electrochemical capacitance properties. *J. Phys. Chem. C* **112**, 4406–4417 (2008).
34. Toupin, M., Brousse, T. & Bélanger, D. Charge storage mechanism of MnO_2 electrode used in aqueous electrochemical capacitor. *Chem. Mater.* **16**, 3184–3190 (2004).
35. Ghodbane, O., Ataherian, F., Wu, N. L. & Favier, F. In situ crystallographic investigations of charge storage mechanisms in MnO_2-based electrochemical capacitors. *J. Power Sources* **206**, 454–462 (2012).
36. Su, Z. et al. Scalable fabrication of MnO_2 nanostructure deposited on free-standing Ni nanocone arrays for ultrathin, flexible, high-performance micro-supercapacitor. *Energy Environ. Sci.* **7**, 2652–2659 (2014).

Acknowledgements

This research is supported in part by grants from the Project of Saitama Prefectural Industry-Accademia Collaborative Development Project Subsidy. J.L. acknowledges support by NSF ECCS-1610806. This research project started in 2015 as a collaborative research project with the laboratory of Mildred S. Dresselhaus (Institute Professor of Massachusetts Institute of Technology). Mildred S. Dresselhaus supervised this research project until she passed away in February 2017.

Author contributions

W.G. and B.F. conceived the idea and designed the experiments. W.G. carried out most of the experimental works. Z.W. and H.O. carried out SEM and XRD. I.S., L.S., X.Z., M. L., C.W., J.L., J.O.-M., M.T., and M.E. discussed the interpretation of results and co-wrote the paper. All authors discussed the results commented on the manuscript.

Additional information

Supplementary information accompanies this paper at https://doi.org/10.1038/s42004-018-0017-z.

Competing interests: The authors declare no competing interests.

Reprints and permission information is available online at http://npg.nature.com/reprintsandpermissions/

Publisher's note: Springer Nature remains neutral with regard to jurisdictional claims in published maps and institutional affiliations.

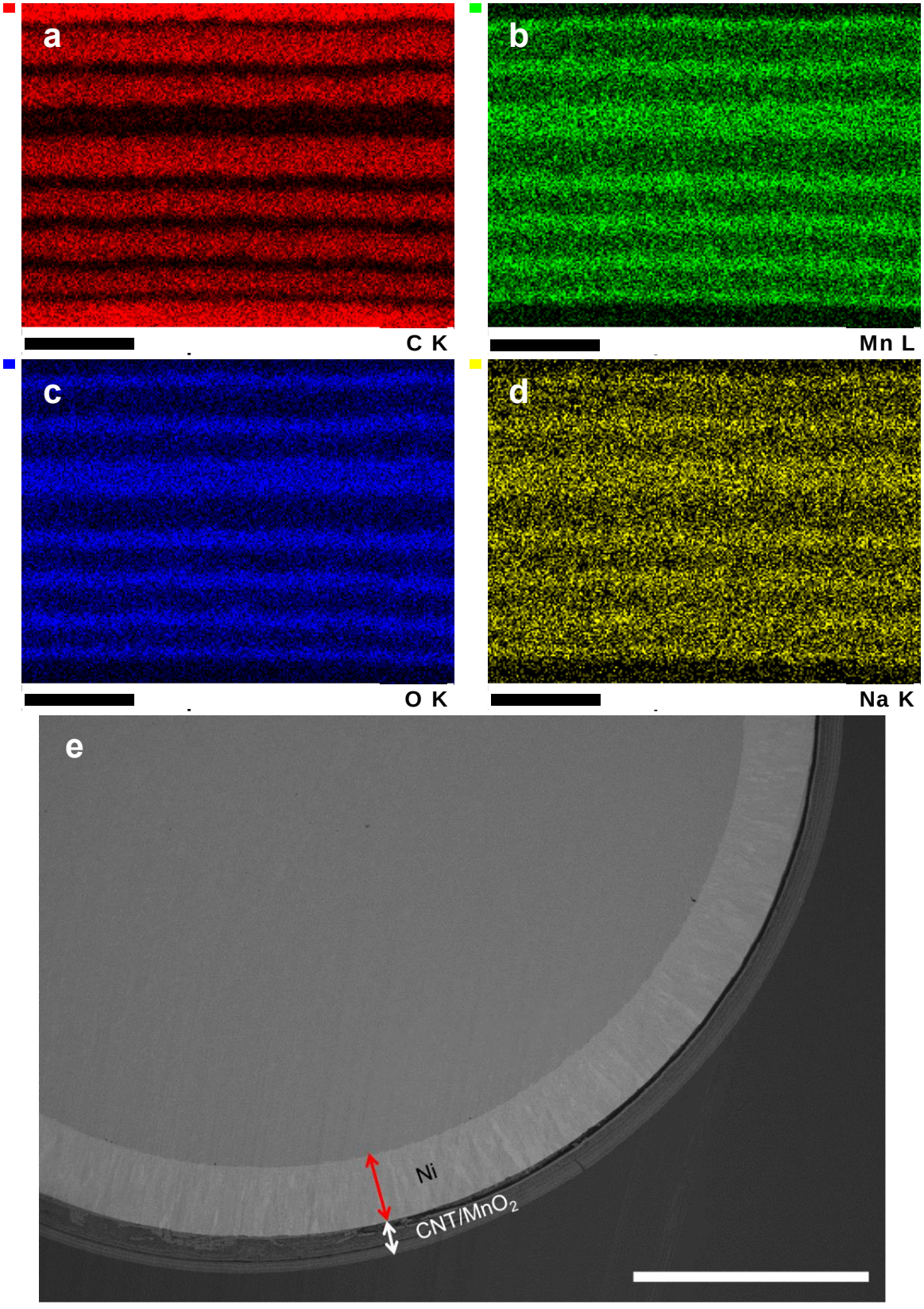

Supplementary Figure 1. Microstructures of a CNT/MnO_2 nanostructured electrode. (a-d) Elemental mapping analyses performed on the cross-section area of a Ni/CNT/MnO_2 electrode and the locations of (a) C (carbon, red dots), (b) Mn (manganese, green dots), (c) O (oxygen, blue dots) and (d) Na (sodium, yellow dots) atoms are spotted (all scale bars, 3 μm); (e) a SEM image of the cross-section area of the same Ni/CNT/MnO_2 electrode at a low resolution (scale bar, 50 μm).

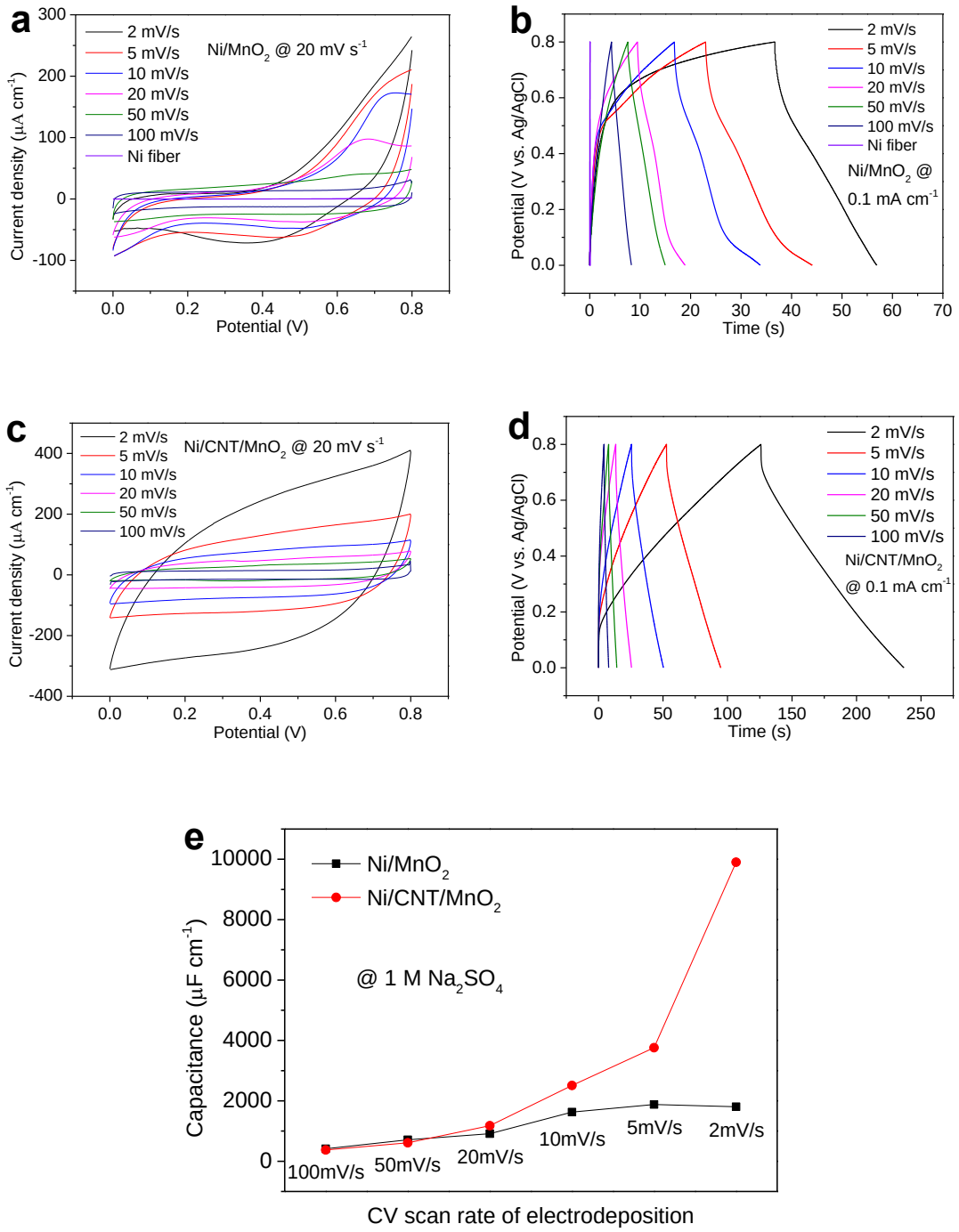

Supplementary Figure 2. Electrochemical performances of the electrodes with and without CNT-networks. (a) CV curves of Ni/MnO_2 (single layered MnO_2 without CNT-networks) electrodes prepared via electrodeposition with the CV scan rate at 2, 5, 10, 20, 50, and 100 mV s^{-1}, respectively. (b) Galvanostatic charge-discharge curves of the same Ni/MnO_2 electrodes at a current density of 0.1 mA cm^{-1}. (c) CV curves of the $Ni/CNT/MnO_2$ (single-layered MnO_2 and single-layered CNT-networks) electrodes prepared via electrodeposition with the identical CV scan rate as in (a) and (d) the coresponding galvanostatic charge-discharge curves at a current density of 0.1 mA cm^{-1}. (e) Comparison of the specific capacitances of the Ni/MnO_2 and the $Ni/CNT/MnO_2$ electrodes prepared by using identical CV scan rate for the electrodeposition of MnO_2.

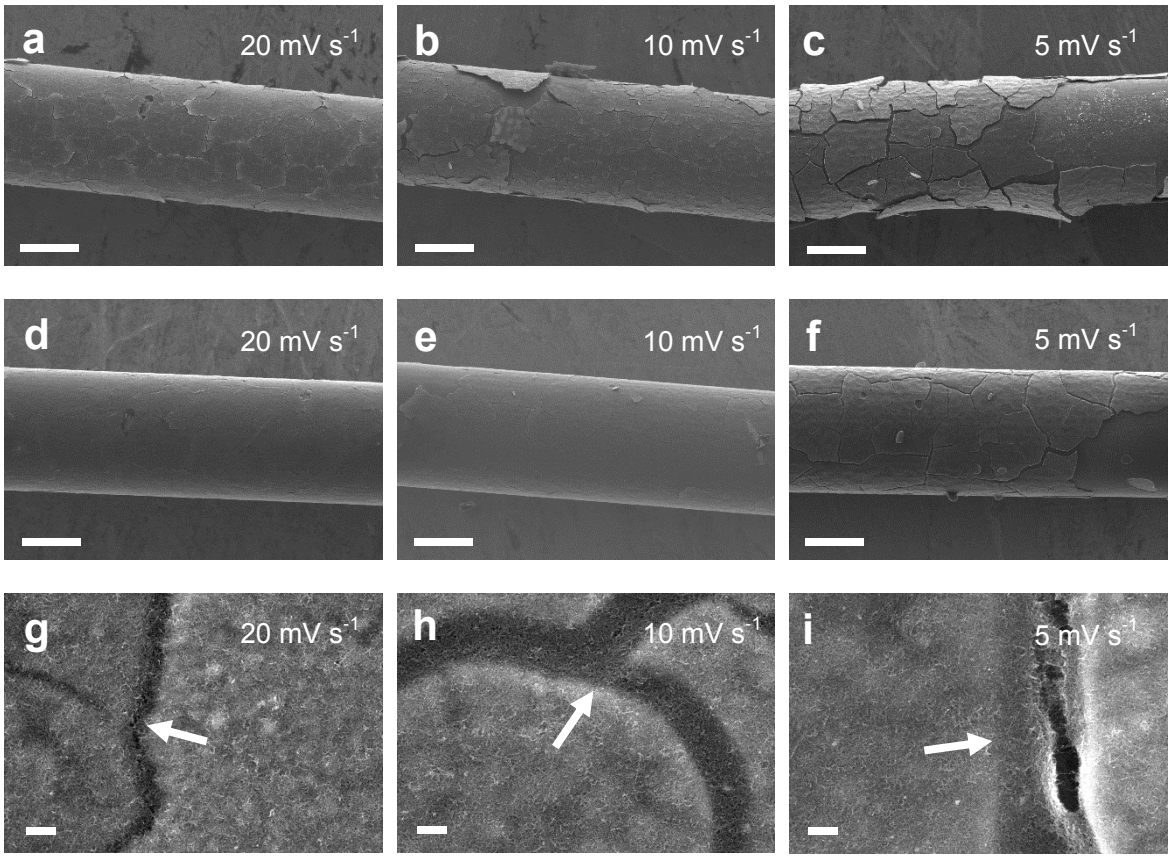

Supplementary Figure 3. SEM images of typical Ni/MnO_2 and $Ni/CNT/MnO_2$ electrodes. Ni/MnO_2 electrodes prepared via electrochemical deposition at CV scan rate of (a) 20 mV s^{-1}, (b) 10 mV s^{-1}, (c) 5 mV s^{-1} (all scale bars, 100 μm). The $Ni/CNT/MnO_2$ electrodes prepared at (d) 20 mV s^{-1}, (e) 10 mV s^{-1}, (f) 5 mV s^{-1} (all scale bars, 100 μm). Magnified SEM images of CNT-networks of the $Ni/CNT/MnO_2$ electrodes (g, h, i) (all scale bars, 1 μm); arrows: cracked MnO_2 domains being wrapped by CNT-networks.

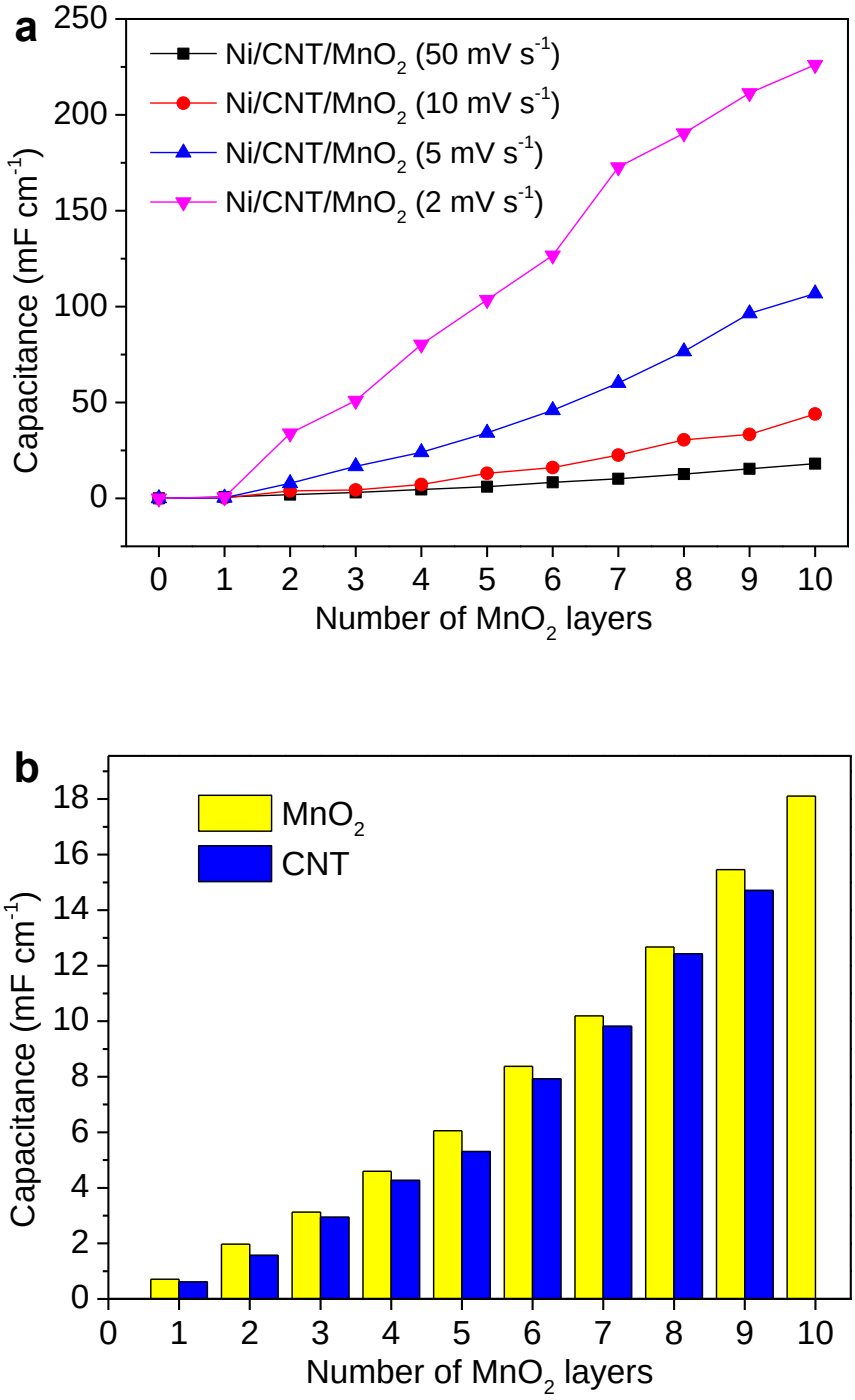

Supplementary Figure 4. Capacitance of the electrodes with different number of MnO_2 layers. (a) Specific capacitance of the Ni/CNT/MnO_2 electrodes *versus* numbers of electrodeposition of MnO_2 domains; each layered MnO_2 domains were electrochemically deposited within the CNT-networks. Ni/CNT/MnO_2 electrodes prepared via electrodeposition with the CV scan rate at 2, 5, 10 and 50 mV s^{-1} are shown in this figure. (b) Specific capacitances of the Ni/CNT/MnO_2 electrodes prepared by using the scan rate at 50 mV s^{-1}; MnO_2 was accumulated from 1 layer to 10 layers, CNT-networks were inserted between each of the MnO_2 layers.

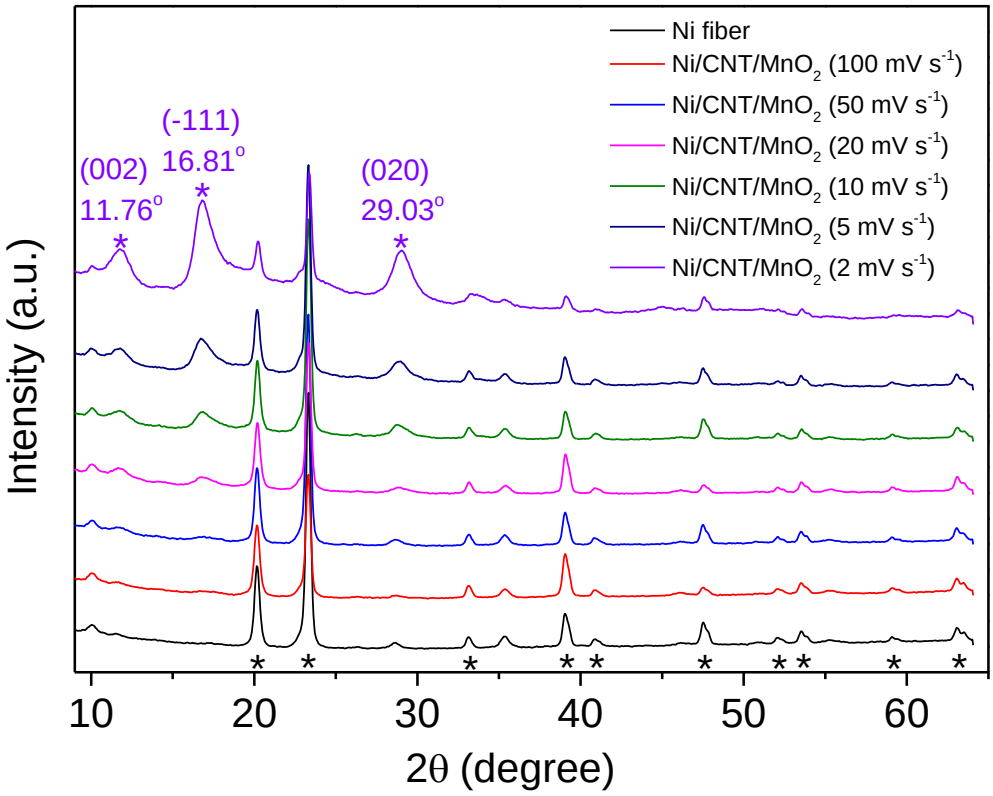

Supplementary Figure 5. Crystal structure of the electrodes. XRD patterns of the typical Ni/CNT/MnO_2 hybrid nanostructured electrodes prepared via electrodeposition at the CV scan rate of 2, 5, 10, 20, 50, and 100 mV s^{-1}, respectively.

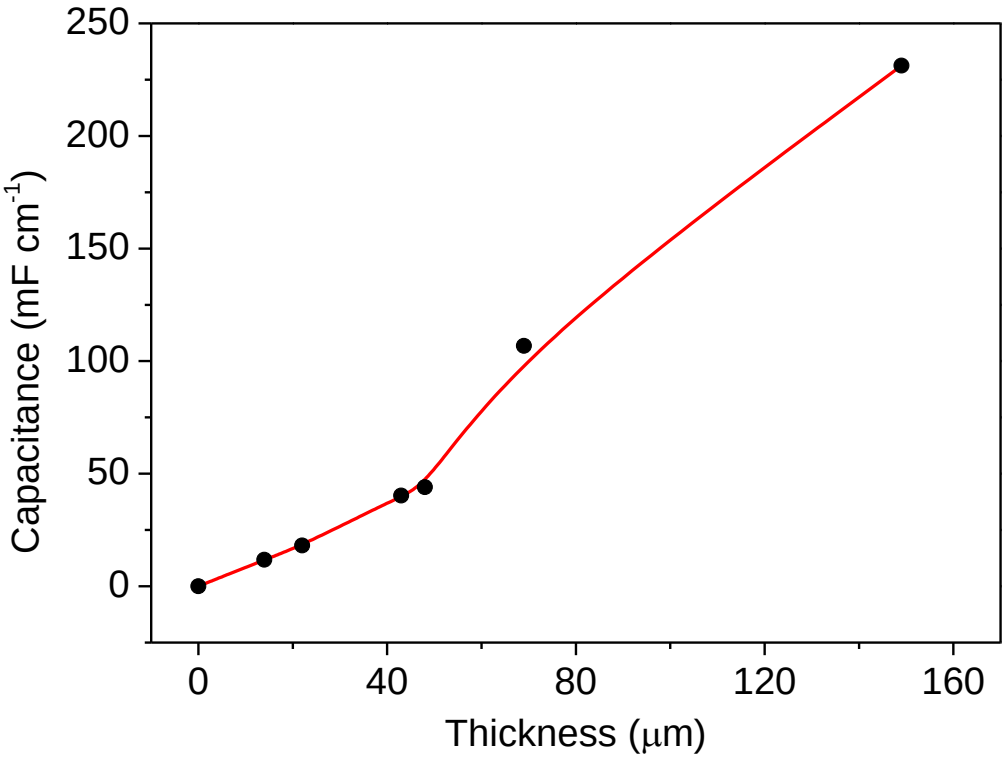

Supplementary Figure 6. Specific capacitance *versus* thickness of the CNT/MnO_2 hybrid nanostructures of the electrodes. The specific capacitances for all electrodes were proportional to the thicknesses of CNT/MnO_2.

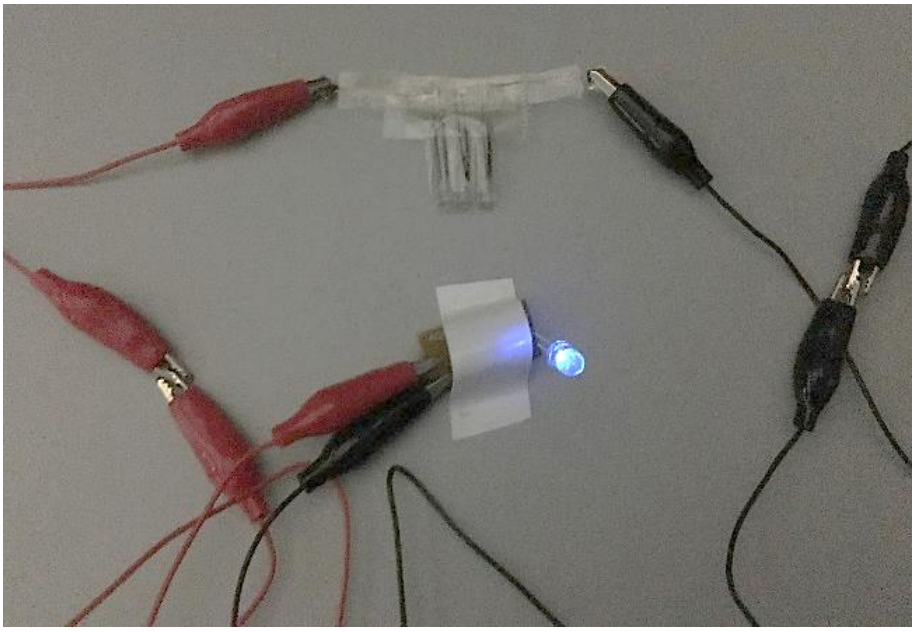

Supplementary Figure 7. Digital photograph of a light-emitting diode (LED) lightened by three fiber supercapacitors connected in parallel. The Ni/CNT/MnO_2 electrodes were the 9-layered MnO_2 and 9-layered CNTs, the thickness of CNT/MnO_2 is 48 μm.

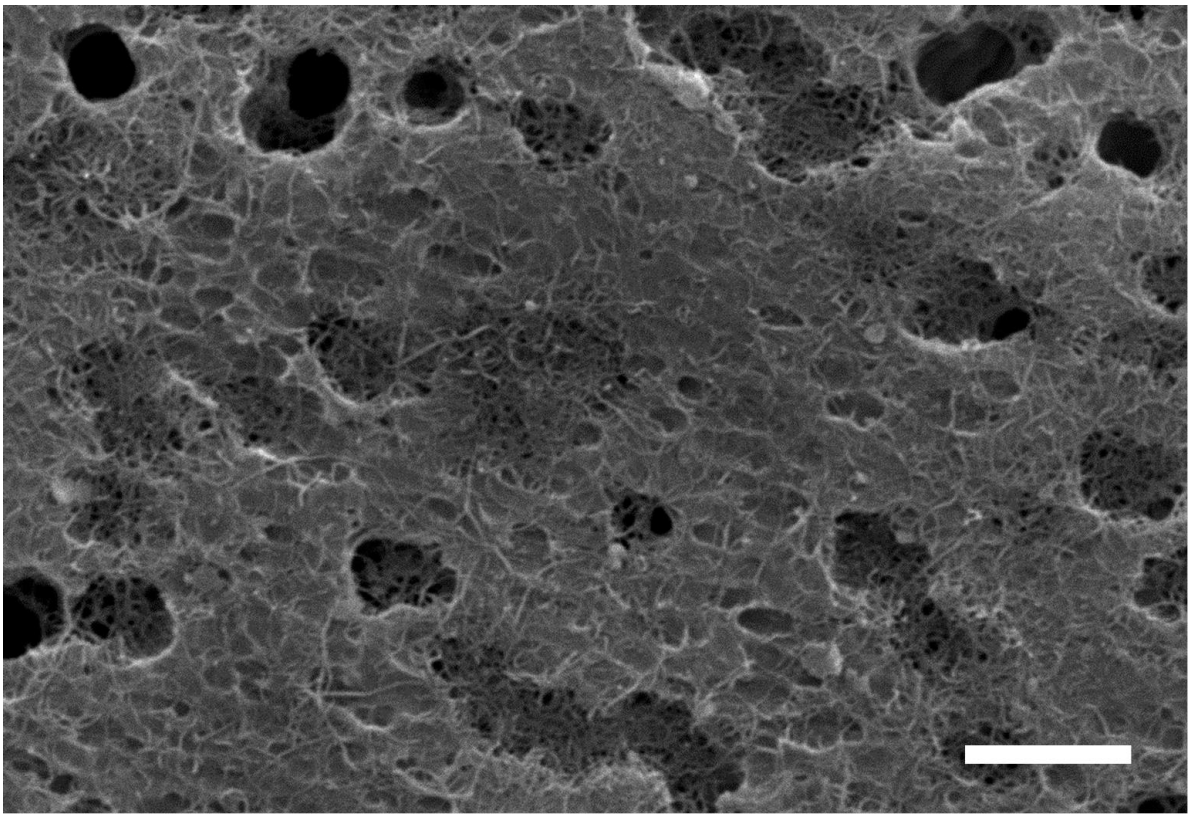

Supplementary Figure 8. A typical SEM image of multi-walled CNTs being dispersed into tubular level of dispersions in water. The dispersion contained 4.0 wt% multi-walled CNTs, which was diluted to 1/1000 with deionized water, filtered by using an alumina based nano-filter, dried in air and then was observed using SEM (scale bar, 2 μm).